

## Analytical Investigation on Fundamental Electrical Characteristics of Large Air-gap Superconducting Synchronous Machine

M. Yazdanian\*, P. Elhaminia, M. R. Zolghadri, and M. Fardmanesh

*Electrical Engineering Department, Sharif University of Technology, Tehran, P.O. Box 11155-8639, Iran*

(Received 5 March 2013, Received in final form 12 June 2013, Accepted 12 June 2013)

**In this paper a general 2-D model of a large air-gap synchronous machine either with non-magnetic or magnetic core rotor is investigated and electrical characteristics of the machine are analytically calculated. Considering the general model, analytical equations for magnetic field density in different regions of the large air-gap machine are calculated. In addition, self and mutual inductances in the proposed model of the machine have been developed, which are the most important parameters in the electromagnetic design and transient analysis of synchronous machines. Finite element simulation has also been performed to verify the obtained results from the equations. Analytical results show good agreement with FEM results.**

**Keywords :** large air-gap machine, Finite Element Modeling (FEM), electromagnetic design of machine, self and mutual inductance calculation, synchronous machine

### 1. Introduction

Synchronous machines are widely employed in high power applications because of their higher efficiency, higher power density, and ability to provide a system power factor improvement. High power density electrical machines will provide important benefits in transportation applications such as ship propulsion systems. Larger flux density of field winding or higher linear current density of the armature leads to higher power density in synchronous machines but both of these parameters are restricted by iron-teeth of the stator [1].

In the air-cored machines, iron teeth of the stator are replaced with non-magnetic support structure. Moreover, in order to decrease the weight of the machine in some topologies, the massive iron rotor is replaced by non-magnetic low-weight structure. Eliminating iron teeth of the machine increases the magnetic reluctance. Therefore, in order to magnetize the machine to the required value, a large amount of magnetomotive force (MMF) is required. The conventional copper field winding cannot provide this MMF due to losses and volume restrictions. Therefore, high temperature superconducting (HTS) tapes can

be used in air-cored machines, which are capable to conduct about 100 times the electrical current of copper wire of the same dimensions without significant losses [2].

The most common structure of superconducting synchronous machine (SSM) is the radial-flux rotating field type machine using the superconducting field winding while the armature winding consists of copper coils fixed by non-magnetic high strength materials such as G10. The field winding can be placed on either magnetic or non-magnetic support structure. Non-magnetic core rotor declines weight and volume but increases the cost of the machine due to higher required length of the superconducting tapes [3, 4].

The critical current of the superconducting tapes decreases significantly in the presence of an external magnetic field especially by the perpendicular components to the broader face of the tape. In addition, variable magnetic field causes vortex losses in superconductors and can change the state of the superconductor to normal. Therefore, a damper screen is placed between armature and field windings in order to protect the HTS field winding against the transient magnetic flux, which increases the air-gap length [5].

The linear current density of the armature winding is restricted by thermal and mechanical considerations of the stator. Furthermore, synchronous reactance of machine

---

©The Korean Magnetism Society. All rights reserved.

\*Corresponding author: Tel: +98 9122138277

Fax: +98 21 66165990, e-mail: m.yazdanian@gmail.com

limits linear current density of the machine. In the air-cored synchronous machine, because of large air-gap, the synchronous reactance of machine is very low, e.g. 0.2 per-unit. Therefore, superconducting machines exhibit better stability compared to the conventional synchronous machines [6]. Due to large air gap of superconducting synchronous machines, the design and magnetic calculations of this kind of machine is quite different from the conventional machines [3].

In the earlier works, the magnetic flux density of a superconducting machine is calculated in two-dimensional plane using a simple model of air-cored machine [7, 8]. In this model the machine consists of stationary armature windings in a smooth bore of stator iron yoke and rotating excitation field winding located on non-magnetic rotor. Basic equations for the simple model of the machine are calculated which determine the distribution of magnetic flux density inside the synchronous air-cored machine. In [9], a new model for superconducting machine is suggested which is capable of representing different types of rotor core. The suggested model of the machine uses a hollow shape core rotor which is depicted in Fig. 1.

In this paper the limitation of conventional synchronous machine are investigated and fundamental equations for design of different types of synchronous superconducting machines are presented. Moreover, the suggested analytical modeling can be used in order to compare different structures of the machine and optimal design process of the machine with respect to the machine parameters such as weight, volume, etc. The results of the analytical modeling are compared to the results of the finite element modeling which show good agreement.

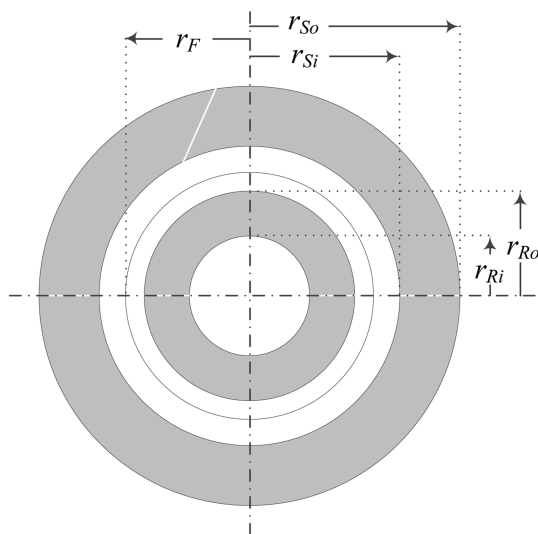


Fig. 1. Schematic of General Machine Model.

## 2. Limitations of Classic Synchronous Machine

In the conventional machines, stator iron-teeth guide the flux toward the back iron and support the armature copper windings. The saturation of the stator iron-teeth limits the radial flux density as follows [1]:

$$B_r = (1 - \lambda_p)B_s \quad (1)$$

where  $\lambda_p$  is the fraction of stator that is dedicated to the stator windings.  $B_s$  and  $B_r$  are saturation level of the magnetic iron and maximum radial flux density of the machine, respectively. The typical scheme of stator magnetic teeth is illustrated in Fig. 2.

The armature windings are placed in the slots between iron-teeth. In order to see the limitation of linear current density of machine, the active power of machine should be investigated. The basic model of synchronous machine is well-known and consists of a voltage source and a synchronous reactance. In order to investigate the active power of the machine, a synchronous machine which is connected to infinite bus-bar can be considered. The per-unit active power of machine connected to infinite bus-bar can be written as follows [1]:

$$p = \frac{ve_f}{x_d} \sin \delta \quad (2)$$

where  $v$ ,  $e_f$ ,  $x_d$  and  $\delta$  are infinite bus-bar per-unit voltage, per-unit internal voltage, per-unit synchronous reactance, and power angle, respectively. Due to transient stability considerations, the power angle is limited to a value between 15 and 25 degrees. In order to increase output power with the limited power angle, the synchronous reactance should be decreased. The synchronous reactance can be written as [1]:

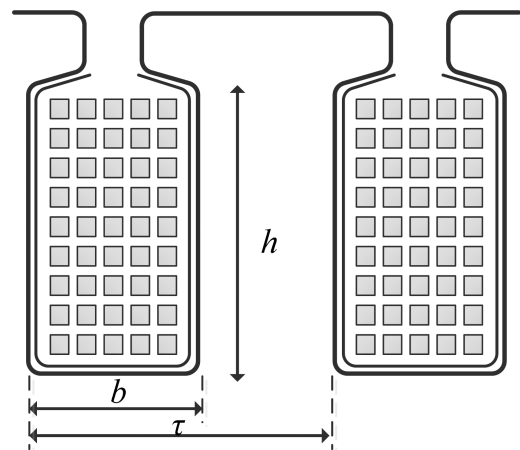


Fig. 2. Typical iron teeth in conventional machines.

$$x_d = \sqrt{2} \frac{\mu_0 r_a k_s}{\rho g} \times \frac{\lambda_p}{1 - \lambda_p} \times \frac{h_s J_a}{B_s} \quad (3)$$

where  $r_a$  is the armature radius,  $k_s$  is the armature winding factor,  $g$  is the air gap length,  $h_s$  is the slot depth and  $J_a$  is the current density in each slot. In order to decrease the synchronous reactance, the air-gap length should be increased. It should be noticed that decreasing the parameter  $h_s J_a$ , which is proportional to the linear current density of machine, does not result in higher power density because the internal voltage of machine is proportional to this parameter too. The larger air gap can be provided by either decreasing the rotor radius or replacing the iron-teeth with non-magnetic materials. Removing the iron-teeth has many advantages such as increasing maximum radial magnetic flux and more filling factor of stator winding because saturation of iron-teeth does not restrict width of the slots. Moreover, the required insulator in the slots are decreased because the non-magnetic teeth are made from high strength non-conductive materials. Therefore, the filling factor of armature winding can be increased. The larger air-gap needs more turn-ampere in the field winding. Therefore, the copper field winding in the air-cored machine decreases the efficiency, while using superconducting tapes can conduct electrical current without significant losses. Consequently, high power air-cored machines should utilize superconductors as the field winding. Therefore, using air-cored superconducting machine has many advantages such as increased efficiency, power system stability, better operation performance and reduced volume and weight in comparison with conventional machines.

### 3. Analysis of Magnetic Flux Density in Air-cored Machines

For conventional machines, magnetic circuit theory is able to calculate the machine magnetic parameters with good precision but for a large air-gap machine, the magnetic circuit is not well definable. Consequently, the magnetic calculation of machine is quite different and makes the design of the superconducting synchronous machines more challenging. Calculation of magnetic flux density distribution in the machine is the fundamental step in electromagnetic design of machine.

In order to calculate the distribution of flux density of different regions inside the machine, a suggested two-dimensional model is considered. The proposed structure and the radii of important regions are depicted in Fig. 1. The field winding is represented by a sinusoidal current sheet in the mean radius of the field winding,  $r_f$ . It is assumed that the sinusoidal current sheet is placed bet-

ween the hollow shape rotor with inner and outer radii  $r_{Ri}$  of  $r_{Ro}$ , and stator iron yoke (magnetic shield) with inner and outer radius of  $r_{Si}$  and  $r_{So}$ , respectively. In such a way, solving Laplace's equation for magnetic vector potential in cylindrical coordination, the radial and the tangential components of magnetic flux density in desired radius  $r$  resulting from a current sheet at the radius of  $r_f$ , have been calculated.

In practice, the field winding is a concentrated winding with a considerable thickness. In [8] it is suggested that desired periodic winding can be represented by Fourier series of sinusoidal current sheets as follows:

$$A_f = \sum_{n=1}^{\infty} \hat{A}_{fn} \sin(np\theta) \quad (4)$$

Then the thickness of the field winding has been taken into account by assuming the winding to be made up from a number of thin current sheets each of thickness of  $dr_f$ , when the linear current density of each sheet is as follows:

$$dA_n = J_{fn} \times dr_f \quad (5)$$

Integration with respect to the thickness of the field winding after substituting  $dA_n$  for  $A_n$  in the radial and tangential magnetic flux density equations, results in the magnetic flux density in desired radius  $r$ . Assuming non-magnetic core rotor, the results of magnetic flux density are presented in [8].

Considering desired linear periodic current sheet, the radial and tangential magnetic flux density for  $n^{\text{th}}$  harmonic inside and outside the field winding region in cylindrical coordination  $(r, \theta)$  are calculated as follows:

$$r < r_f : \begin{Bmatrix} B_{rn} \\ B_{\theta n} \end{Bmatrix} = \frac{\mu_0 A_n}{2} \sigma_{ri, \theta i} \left(\frac{r_f}{r}\right)^{np+1} \begin{Bmatrix} \cos(np\theta) \\ -\sin(np\theta) \end{Bmatrix} \quad (6)$$

$$r > r_f : \begin{Bmatrix} B_{rn} \\ B_{\theta n} \end{Bmatrix} = \frac{\mu_0 A_n}{2} \sigma_{ri, \theta i} \left(\frac{r_f}{r}\right)^{np+1} \begin{Bmatrix} \cos(np\theta) \\ -\sin(np\theta) \end{Bmatrix} \quad (7)$$

where  $\mu_0$ ,  $A$ , and  $\sigma$  are permeability in free space, current sheet density of sinusoidal field winding and influence of iron in the structure of machine, respectively. Using new boundary conditions, the  $\sigma$  parameter in (3) and (4), are calculated as follows:

$$\sigma_{ri, \theta i} = \frac{\left(1 + \eta_S \lambda_S \left(\frac{r_f}{r_{Si}}\right)^{2np}\right) \left(1 \pm \eta_R \lambda_R \left(\frac{r_f}{r_{Si}}\right)^{2np}\right)}{1 - \eta_S \lambda_S \eta_R \lambda_R \left(\frac{r_f}{r_{Si}}\right)^{2np}} \quad (8)$$

$$\sigma_{r_o, \theta_o} = \frac{\left(1 + \eta_S \lambda_S \left(\frac{r_f}{r_{Si}}\right)^{2np}\right) \left(1 + \eta_R \lambda_R \left(\frac{r_f}{r_{Si}}\right)^{2np}\right)}{1 - \eta_S \lambda_S \eta_R \lambda_R \left(\frac{r_f}{r_{Si}}\right)^{2np}} \quad (9)$$

Considering  $\mu_S$  and  $\mu_R$  as stator and rotor relative permeability respectively,  $\mu_S, \mu_R, \lambda_S$  and  $\lambda_R$  are defined as:

$$\lambda_S = \frac{\mu_S - 1}{\mu_S + 1}, \quad \eta_S = \frac{1 - \left(\frac{r_{Si}}{r_{So}}\right)^{2np}}{1 - \lambda_S^2 \left(\frac{r_{Si}}{r_{So}}\right)^{2np}} \quad (10)$$

$$\lambda_R = \frac{\mu_R - 1}{\mu_R + 1}, \quad \eta_R = \frac{1 - \left(\frac{r_{Ri}}{r_{Ro}}\right)^{2np}}{1 - \lambda_R^2 \left(\frac{r_{Ri}}{r_{Ro}}\right)^{2np}} \quad (11)$$

It should be mentioned that in this paper upper and lower signs are considered to be associated to the radial and the tangential components of magnetic field respectively.

In order to consider both non-sinusoidal distribution and the thickness of the field winding, following integration with respect of the field current sheet thickness should be calculated.

$$B_{r_n, \theta_n} = \int_{r_{fi}}^{r_{fo}} dB_{r_n, \theta_n} dr_f \quad (12)$$

There are five important regions in the simplified model of the machine as follows:

- 1) *Region I*: The magnetic or non-magnetic core rotor.
- 2) *Region II*: The region between rotor core and field winding.
- 3) *Region III*: The region between inner and outer radii of field winding.
- 4) *Region IV*: The region between field winding and magnetic stator.
- 5) *Region V*: The stator iron core.

For the desired point inside regions *I* and *II*, (3) should be substituted in (9), but in regions *IV* and *V*, (4) should be substituted in (9). Whenever the desired point is located in region *III*, the magnetic flux density can be calculated using superposition law. Therefore, magnetic flux density in this region can be written as follows:

$$B_{r_n, \theta_n} = \int_{r_{fi}}^r dB_{r_n, \theta_n} dr_f + \int_r^{r_{fo}} dB_{r_n, \theta_n} dr_f \quad (13)$$

where  $B_{r_n, \theta_n}$  in the first and second term should be substituted from (4) and (3) respectively. Solving these integrations yields the magnetic flux density distribution in desired point but  $np = 2$  results in an indeterminate form, where  $n$  is the harmonic order and  $p$  is the pole pair numbers. The results for  $np = 2$  can be converted to a determinate form using L'Hopital's rule. The maximum values of the calculated radial and tangential magnetic flux densities of different harmonics are presented in Table 1.

**Table 1.** Radial and tangential magnetic flux densities in different regions.

Region	Magnetic Flux Density ( $np \neq 2$ )
<i>Reg. I</i> $r_{ri} < r < r_{ro}$	$\hat{B}_{in,n} = \frac{\pm \mu_0 \hat{J}_{in}}{2(1-\beta)} r \left(\frac{r}{r_{fo}}\right)^{np-2} (1 + \eta_R \lambda_R) \left(\frac{1 - \eta_R \left(\frac{r_{Ri}}{r}\right)^{2np}}{1 - \eta_R \left(\frac{r_{Ro}}{r}\right)^{2np}}\right) \left(\mathcal{K} + \eta_S \lambda_S \left(\frac{r_{fo}}{r_{si}}\right)^{2np} \mathcal{H}\right)$
<i>Reg. II</i> $r_{ro} < r < r_{fi}$	$\hat{B}_{in,n} = \frac{\pm \mu_0 \hat{J}_{in}}{2(1-\beta)} r \left(\frac{r}{r_{fo}}\right)^{np-2} \left(1 \pm \eta_R \lambda_R \left(\frac{r_{Ro}}{r}\right)^{2np}\right) \left(\mathcal{K} + \eta_S \lambda_S \left(\frac{r_{fo}}{r_{si}}\right)^{2np} \mathcal{H}\right)$
<i>Reg. III</i> $r_{fi} < r < r_{fo}$	$\hat{B}_{f,n} = \hat{B}_{out,n} _{r_{fo}=r} + \hat{B}_{in,n} _{r_{fi}=r}$
<i>Reg. IV</i> $r_{fo} < r < r_{si}$	$\hat{B}_{out,n} = \left(\frac{r_{fo}}{r}\right)^{np+2} \left(1 \pm \eta_S \lambda_S \left(\frac{r}{r_{si}}\right)^{2np}\right) \left(\eta_R \lambda_R \left(\frac{r_{Ro}}{r_{fo}}\right)^{2np} \mathcal{K} + \mathcal{H}\right)$
<i>Reg. V</i> $r_{si} < r < r_{so}$	$\hat{B}_{out,n} = \frac{\mu_0 \hat{J}_{in}}{2(1-\beta)} r \left(\frac{r_{fo}}{r}\right)^{np+2} (1 + \eta_S \lambda_S) \left(\frac{1 - \eta_S \left(\frac{r}{r_{so}}\right)^{2np}}{1 - \eta_S \left(\frac{r_{Si}}{r_{so}}\right)^{2np}}\right) \left(\eta_R \lambda_R \left(\frac{r_{Ro}}{r_{fo}}\right)^{2np} \mathcal{K} + \mathcal{H}\right)$
	$\beta = \eta_S \lambda_S \eta_R \lambda_R \left(\frac{r_{Bo}}{r_{Si}}\right)^{2np}$ $\chi = \frac{\mu_0 \hat{J}_{in}}{2(1-\beta)} r$ $\mathcal{K} = \frac{1 - \left(\frac{r_{fi}}{r_{fo}}\right)^{2-np}}{2 - np}$ $\mathcal{H} = \frac{1 - \left(\frac{r_{fi}}{r_{fo}}\right)^{2+np}}{2 + np}$

\*The upper and lower signs belong to the radial and tangential component of magnetic field

**Table 2.** Units for magnetic properties.

Symbol	Quantity	Value (unit)
$S$	apparent power of machine	300 kVA
$n_{sync}$	synchronous speed	250 rpm
$p$	pole-pair numbers	3
$r_{Ri}$	inner radius of rotor	160 mm
$r_{Ro}$	outer radius of rotor	245 mm
$r_{fi}$	inner radius of field winding	250 mm
$r_{fo}$	outer radius of field winding	270 mm
$r_{ai}$	inner radius of armature winding	300 mm
$r_{ao}$	outer radius of armature winding	340 mm
$r_{Si}$	inner radius of magnetic shield	345 mm
$r_{So}$	outer radius of magnetic shield	430 mm
$j_f$	current density of field winding	170 A/mm <sup>2</sup>
$\delta_i$	inner angle of field winding	20 degrees
$\delta_o$	outer angle of field winding	28 degrees
$\mu$	relative permeability of rotor and stator core	1000

In order to investigate the analytical results, the magnetic flux density of field winding is compared with Finite Element Model (FEM) of a simple synchronous superconducting machine. Therefore, a typical low speed 300 kVA machine with constant permeability for ferromagnetic components is considered. The parameters of the typical machine are given in Table 2. For simplicity of calculation, it is assumed that the field winding is placed in curvy quadrilateral, which is bounded by two arcs of concentric circles and two radii of the circles. The simplified model and field winding parameters are shown in Fig. 3. The abovementioned filed winding can simply be represented by Fourier series as follows:

$$J_n = \frac{4J}{n\pi}(\cos(np\delta_i) - \cos(np\delta_o)) \quad (14)$$

Using equations of Table 1 and (14), the analytical calculations for the typical machine have been performed

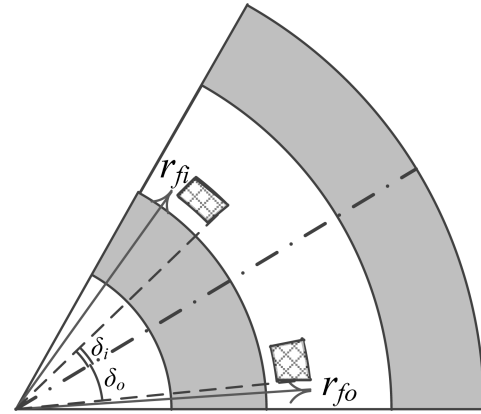


**Fig. 3.** The simplified model of machine with iron rotor.

up to the 13th harmonic. As can be seen in Fig. 4, the analytical results and the FEM results are in close agreement. For instance the comparison of analytical and FEM result in Region II for both radial and tangential component of magnetic flux is depicted in Fig. 4. The source of the error between the analytical results and the FEM results is limited number of harmonics that counted in calculations and the precision of FEM, which depends on parameters such as mesh quality.

### 4. Inductances of Machine

In the conventional machine, the inductances of machine can be adjusted by the air-gap value but in an efficient air-cored machine design algorithm, the number of turns of armature and field windings should be selected properly to achieve desired value of inductances. Therefore accurate calculation of machine inductances leads to better design and optimization process.

Calculations of machine inductances are based on magnetic energy stored in the coils. The stored energy in

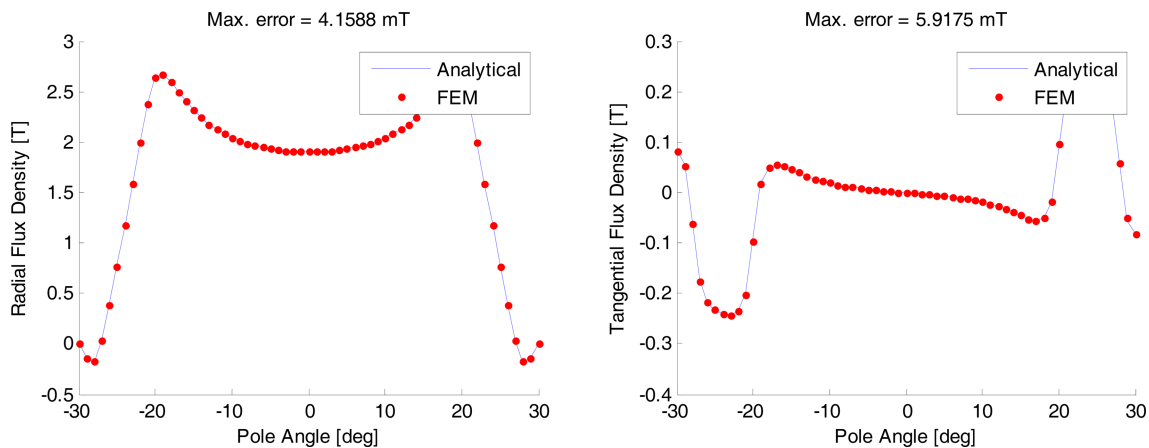


**Fig. 4.** (Color online) Comparison of analytical and FEM result in Region II.

a coil can be written as follows [10]:

$$W_m = \frac{1}{2} LI^2 \quad (15)$$

On the other hand, the magnetic energy can be derived by integrating the product of magnetic vector potential and the current density over all space as follows [11]:

$$W_m = \frac{1}{2} \int_V \vec{\psi} \cdot \vec{J} dv' \quad (16)$$

It should be noticed that only one winding is energized and the others should be considered non-excited. Therefore, the integration volume is restricted to coil volume and the self-inductance on each winding can be calculated using following equation:

$$L = \frac{\int_V \vec{\psi} \cdot \vec{J} dv'}{I^2} \quad (17)$$

where  $V'$  is the volume of coil windings. The same method is used for calculating the mutual inductance as follows:

$$W_{m,12} = M_{12} I_1 I_2 \quad (18)$$

$$W_{m,12} = \int_{V'} \vec{\psi}_1 \cdot \vec{J}_2 dv' \quad (19)$$

Using abovementioned method, the self and mutual inductances are derived. Defining the armature radius ratio and ( $x = r_{fi}/r_{fo}$ ) the field radius ratio ( $y = r_{ai}/r_{ao}$ ), the self-inductance of armature winding and field winding can be written as:

$$L_a = \sum_{\substack{n=1 \\ n \text{ odd}}}^h \frac{8\mu_0 l_a (k_a k_{wa} N_a)^2}{n \pi p (1-x^2)} \mathcal{L}_n(x, r_{ao}) \quad (20)$$

$$L_f = \sum_{\substack{n=1 \\ n \text{ odd}}}^h \frac{8\mu_0 l_f (k_f N_a)^2}{n \pi p (1-y^2)} \mathcal{L}_n(y, r_{fo}) \quad (21)$$

where

$$\mathcal{L}_n(\mathcal{G}, r) = \frac{P_1 + P_2 + P_3 + P_4}{(1-\beta)}$$

$$P_1 = \frac{(\beta + y^2)}{2(2-np)} + \frac{(1 + \beta \mathcal{G}^2)}{2(2+np)}$$

$$P_2 = -\frac{2\mathcal{G}^{2+np}}{(4-n^2 p^2)} - \frac{2\beta \mathcal{G}^{2-np}}{(4-n^2 p^2)}$$

$$P_3 = \frac{(1 - \mathcal{G}^{2+np})^2}{(2+np)^2} \eta_s \lambda_s \left(\frac{r}{r_{si}}\right)^{2np}$$

$$P_4 = \frac{(1 - \mathcal{G}^{2-np})^2}{(2-np)^2} \eta_r \lambda_r \left(\frac{r_{Ro}}{r}\right)^{2np}$$

The mutual inductance between armature and field windings can be written as:

$$M_{af} = \sum_{\substack{n=1 \\ n \text{ odd}}}^h \frac{8\mu_0 l_a k_a k_{wa} N_a k_f N_f \left(\frac{r_{fo}}{r_{ao}}\right)^{np}}{n \pi p (1-x^2)(1-y^2)} \mathcal{M}_n(x, y) \quad (22)$$

where

$$\mathcal{M}_n(x, y) = \frac{T_1 T_2}{(1-\beta)}$$

$$T_1 = \frac{1-y^{2+np}}{(4-n^2 p^2)} + \frac{(1-y^{2-np})}{(2-np)^2} \eta_R \lambda_R \left(\frac{r_{Ro}}{r_{fo}}\right)^{2np}$$

$$T_2 = \frac{1-x^{2-np}}{(4-n^2 p^2)} + \frac{(1-x^{2+np})}{(2+np)^2} \eta_S \lambda_S \left(\frac{r_{ao}}{r_{si}}\right)^{2np}$$

The self and mutual inductances are calculated using abovementioned equations. Besides the self and mutual inductances calculations, they are estimated by finite element method. The analytical and FEM results are compared in Table 3. As can be seen in this table the analytical and FEM results are in good agreement.

As mentioned before, the superconductor winding is surrounded by a cylinder shield (damper) made of a conductive material such as copper or aluminum in order to minimize AC harmonic field experienced by the field winding. The inductance of shield can be calculated using

**Table 3.** Inductances of machine

Symbol	Quantity	Analytical	FEM
$L_f$	Self-inductance of field windings	20.6232	20.6254
$L_a$	Self-inductance of “phase a” of armature winding	0.4831	0.4833
$M_{ab}$	Mutual inductance between “phase a” and “phase b”	0.1849	0.1849
$M_{af}$	Mutual inductance between “phase a” and field winding	2.1701	2.2584
$M_{bf}$	Mutual inductance between “phase b” and field winding	1.1508	1.0631

All conductors are consider to be in series

same equation as (21) or (22), assuming the shield is a single turn coil, which cover whole of pole area. In the same manner, the mutual inductances between field and shield ( $M_{sf}$ ) and between armature and shield ( $M_{sa}$ ) can be calculated.

### 5. Parameter Calculation

Superconducting machines can be characterized using (d-q) axis representation similar to conventional machines. Therefore, different parameters of machine such as transient and sub-transient reactances and time constants of both d-axis and q-axis should be calculated. For a  $N_{ph}$  phase machine, the d-axis and q-axis synchronous reactance can be written as follows [12]:

$$X_d = X_q = \frac{N_{ph}}{2} \omega L_a \quad (23)$$

Transient reactance of d-axis is given by:

$$X_d' = \frac{N_{ph}}{2} \left( X_a - \frac{X_{af}^2}{X_f} \right) \quad (24)$$

The d-axis and q-axis subtransient reactances of machine can be obtained, respectively as follows:

$$X_d'' = \frac{N_{ph}}{2} \left( X_a - \frac{X_s X_{af}^2 - 2 X_{af} X_{as} X_{fs} + X_f X_{as}^2}{X_s X_f - X_{fs}^2} \right) \quad (25)$$

$$X_q'' = \frac{N_{ph}}{2} \left( X_a - \frac{X_{as}^2}{X_s} \right) \quad (26)$$

The armature time constant can be expressed as follows:

$$\tau_a = \frac{1}{\omega r_a} \left( \frac{2}{(1/X_d'') + (1/X_q'')} \right) \quad (27)$$

where  $r_a$  is resistance of armature winding. The transient open-circuit and short-circuit time constants of d-axis are given by:

$$\tau_{do}' = \frac{X_f}{\omega r_f} \quad (28)$$

$$\tau_d' = \frac{1}{\omega r_f} \left( X_f - \frac{X_{af}^2}{X_a} \right) \quad (29)$$

where  $r_f$  is resistance of field winding. As can be seen in (28) and (29), the transient time constants of d-axis are a function of field resistance. According to E-J law equations, the resistance of superconducting field is negligible in comparison with internal resistance of field excitation system including leads and brushes. Therefore, the resistance of field winding can be estimated by resistance of

field excitation system. The subtransient open-circuit and short-circuit time constants of d-axis are as follows:

$$\tau_{do}'' = \frac{1}{\omega r_s} \left( X_s - \frac{X_{sf}^2}{X_f} \right) \quad (30)$$

$$\tau_d'' = \frac{1}{\omega r_s} \left( X_s - \frac{X_f X_{as}^2 - 2 X_{af} X_{as} X_{fs} + X_a X_{fs}^2}{X_a X_f - X_{fa}^2} \right) \quad (31)$$

where  $r_s$  is resistance of shield. The subtransient open-circuit and short-circuit time constants of q-axis can be obtained from:

$$\tau_{qo}'' = \frac{X_s}{\omega r_s} \quad (32)$$

$$\tau_q'' = \frac{1}{\omega r_s} \left( X_s - \frac{X_{as}^2}{X_a} \right) \quad (33)$$

### 6. Conclusion

General equations of radial flux large air-gap machines were derived which can be used to design different structures of superconducting synchronous machines. Using the developed model and relations, the magnetic flux of field winding in different regions of the machine was calculated. Moreover, the self and mutual inductances between machine windings are calculated. The comparison of the derived equations and the FEM results of the typical superconducting machine based on suggested model are in good agreement. The equations can also be used to compare different structure of superconducting machines. In addition, the developed equations can be used in the design and optimization of the machines.

### References

- [1] J. Kirtley and F. Edeskuty, Proceedings of the IEEE **77**, (1989) pp. 1143-1154.
- [2] J. Bumby, Superconducting Rotating Electrical Machines. Clarendon Press, Oxford (1983).
- [3] S. Minnich, T. Keim, M. Chari, B. B. Gamble, M. J. Jefferies, D. Jones, E. T. Laskaris, and P. A. IEEE Trans. Magn. **15**, 703 (1979).
- [4] Kalsi, Applications of High Temperature Superconductors to Electric Power Equipment, Wiley-IEEE (2011).
- [5] H. M. Kim, Y. S. Yoon, Y. K. Kwon, Y. C. Kim, S. H. Lee, J. P. Hong, J. B. Song, and H. G. Lee, IEEE Trans. Appl. Supercond. **19**, 1683 (2011).
- [6] Y. Mitani, K. Tsuji, and Y. Murakami, IEEE Trans. Magn. **27**, 2349 (1991).
- [7] J. L. Kirtley, Proceedings of the IEEE **81** (1993) pp. 449-461.

- [8] S. K. Safi and J. R. Bumby, IEE Proceedings C **139**, Sep 1992.
- [9] M. Yazdani, P. Elhaninia, M. R. Zolghadri, and M. Fardmanesh, IEEE Trans. Appl. Supercond. **23**, 5200406 (2013).
- [10] K. R. Davey and B. B. Gamble, IEEE Trans. Magn. **41**, 2391 (2005).
- [11] David K. Cheng, Field and Wave Electromagnetics, Addison-Wesley, 2nd Ed., Cambridge, MA (1989).
- [12] J. Pyrhoenen, T. Jokinen, and V. Hrabovcova, Design of Rotating Electrical Machines, John Wiley & Sons (2008).